Robust Pore Size Analysis of Filamentous Networks from Three-Dimensional Confocal Microscopy

Walter Mickel,* Stefan Münster,† Louise M. Jawerth,‡ David A. Vader,‡ David A. Weitz,‡ Adrian P. Sheppard,§ Klaus Mecke,* Ben Fabry,† and Gerd E. Schröder-Turk*

*Institut für Theoretische Physik, and †Center for Medical Physics and Technology, Biophysics Group, Friedrich-Alexander Universität Erlangen-Nürnberg, Erlangen, Germany; ‡Experimental Soft Condensed Matter Group, Harvard University, Cambridge, Massachusetts; and §Department of Applied Mathematics, Research School of Physical Science and Engineering, The Australian National University, Canberra, Australia

ABSTRACT We describe a robust method for determining morphological properties of filamentous biopolymer networks, such as collagen or other connective tissue matrices, from confocal microscopy image stacks. Morphological properties including pore size distributions and percolation thresholds are important for transport processes, e.g., particle diffusion or cell migration through the extracellular matrix. The method is applied to fluorescently labeled fiber networks prepared from rat-tail tendon and calf-skin collagen, at concentrations of 1.2, 1.6, and 2.4 mg/ml. The collagen fibers form an entangled and branched network. The medial axes, or skeletons, representing the collagen fibers are extracted from the image stack by threshold intensity segmentation and distance-ordered homotopic thinning. The size of the fluid pores as defined by the radii of largest spheres that fit into the cavities between the collagen fibers is derived from Euclidean distance maps and maximal covering radius transforms of the fluid phase. The size of the largest sphere that can traverse the fluid phase between the collagen fibers across the entire probe, called the percolation threshold, was computed for both horizontal and vertical directions. We demonstrate that by representing the fibers as the medial axis the derived morphological network properties are both robust against changes of the value of the segmentation threshold intensity and robust to problems associated with the point-spread function of the imaging system. We also provide empirical support for a recent claim that the percolation threshold of a fiber network is close to the fiber diameter for which the Euler index of the networks becomes zero.

INTRODUCTION

Most adherent cells within living organisms are surrounded by a three-dimensional connective tissue matrix. Some fundamental cell functions such as the formation of adhesion contacts, cell shape, migration, contraction, and differentiation sensitively depend on the morphology, composition, and mechanical properties of the surroundings (1–3). Yet for convenience and reproducibility of the observations, cells are traditionally cultured on two-dimensional hard plastic or glass culture dishes. This often limits the physiological relevance of the data.

To study cell behavior in a physiologically more relevant three-dimensional environment, reconstituted connective tissue gels are gaining widespread usage (3–5). To produce them, animal tissue is harvested and dissolved, the proteins are then purified and later repolymerized in a cell culture dish. Recipes differ widely for each of these steps, as do the resulting properties of the reconstituted gels.

Structural and morphological characteristics of these networks are important for their mechanical properties and biological functionality. The size of the pores of the fluid phase between the fibers is an important factor for determining the migration behavior of cells (such as cancer cells, neutrophils, smooth muscle cells, or fibroblasts) through the gel (3,4,6,7). The pore size of collagen foams has also been linked to hepatocyte function (8). The relationship between fiber orientation on the one hand and elastic properties on the other hand is the subject of ongoing research (2,9).

In this work, we discuss a conceptually robust definition for a pore or mesh size measure of the fluid phase in biopolymer networks and discuss algorithms to compute it for experimental data sets. Despite the relevance of this quantity, a generic definition and a robust method to extract pore sizes from experimental three-dimensional microscopy data sets have been lacking. Here we discuss the definition of two generic pore size measures based on the so-called (maximal) covering radius transform and on percolation analysis. Both approaches have been successfully applied to the analysis of pore sizes of porous materials, such as sandstones (10–12).

Previous pore-size estimates of biological fiber networks were derived, for example, from observations of collagen volume fraction and fiber radius under the assumption that the network geometry is described by a specific model for random fibers (7,13). Other approaches include Fourier spectra analyses of three-dimensional confocal microscopy images, e.g., of fibrin (14), or from statistical analysis of nearest points on collagen fibers in sections of confocal microscopy image stacks (15), and the analysis of spheres diffusing through the network (16). In contrast to those approaches, our method is based on the analysis of the entire

Submitted April 24, 2008, and accepted for publication September 5, 2008.

Walter Mickel and Stefan Münster contributed equally to this work.

Address reprint requests to Gerd E. Schroeder-Turk, E-mail: gerd.schroeder-turk@physik.uni-erlangen.de.

Editor: Gaudenz Danuser.

0006-3495/08/12/6072/09 $2.00

doi: 10.1529/biophysj.108.135939

three-dimensional real-space network geometry and does not rely on specific assumptions or network models.

We apply our method to confocal microscopy data sets of collagen networks obtained after fluorescently labeling the connective tissue proteins before polymerization. The collagen fibers are represented as thinned skeletal center lines, so-called medial axes, of the high-intensity phase of the binarized data sets. Medial representations are well known in analysis of porous media (17) and medical images (18) and have also been used as representations of collagen networks (19). Here we show that the covering radius transform and the percolation analysis yield intuitive and fundamental measures of pore sizes that are robust if analyzed on the medial axis representation of the collagen fibers.

Moreover, these measures are generic in the sense that they apply to networks of arbitrary geometry and topology (entangled, branched, cross-linked, straight, or curved edges, connected or disconnected, isotropic or anisotropic, homogeneous or heterogeneous). The method is robust against variations of the image analysis parameters, in particular the segmentation threshold.

METHODS

Reconstituted collagen networks from calf-skin collagen and rat-tail tendon were fluorescently labeled and imaged by confocal microscopy with x and y pixel dimension of 0.1 μm and distance of 0.1 μm between consecutive images. The resulting three-dimensional grayscale data sets were transformed into binary data sets using standard threshold-segmentation after smoothing by anisotropic diffusion (20). A line representing the collagen fibers was extracted from the binary data sets as the medial axis of the collagen phase. The pore size distributions and percolation thresholds of the fluid phase were computed from the medial axis of the fluid phase, described in detail in Morphological Image Analysis. Importantly, for these computations the fluid phase was not represented by the complement of the collagen phase in the segmented data set but by the complement of the single-voxel thick medial axis representing the collagen fibers. This approach takes into account that the width of the collagen fibers is ~0.15 μm (7); a wider appearance of the fibers in the segmented data set is mostly due to the point-spread function of the confocal microscopy imaging system.

Synthesis of labeled collagen networks

Acid-soluble calf-skin collagen at 4 mg/mL (Biochrom, Berlin, Germany) and acid-dissolved rat-tail tendon collagen at 2 mg/mL (Biochrom) were each fluorescently labeled with 5-(and 6)-carboxytetramethylrhodamine succinimidyl ester (TAMRA SE, Invitrogen, Carlsbad, CA). We followed the protocol by Baici et al. (21) but used TAMRA SE instead of FITC and omitted the final separation step. To reduce structural alterations due to changes in the dynamics of the network self-assembly, the labeled collagen solutions were each diluted with their unlabeled stock solutions at a volume ratio of 1:4.

Next, the components were mixed in the following order by pipetting: 350-μL labeled calf-skin collagen, 350-μL labeled rat-tail tendon collagen, 80-μL 10× Dulbecco's modified Eagle's medium (DMEM, Sigma, St. Louis, MO), 80-μL 0.25 M sodium bicarbonate, and 13-μL 1 M sodium hydroxide. Care was taken to avoid bubbles and all components were kept on ice before mixing.

The resulting mixture had a collagen concentration of 2.4 mg/mL at a pH of 10. For gels with lower collagen concentration (1.6 mg/mL and 1.2 mg/mL), this mixture was diluted with 1× DMEM adjusted to pH 10. A quantity of 200 μL of the mixture were immediately pipetted into 35-mm glass-bottom culture dishes (MatTek, Ashland, MA) and incubated for 2 h at 37°C. Before confocal imaging, the gels were thoroughly washed with warmed 1× phosphate buffered saline (PBS, Sigma, St. Louis, MO) to eliminate unbound dye or nonpolymerized labeled collagen from the fluid phase.

Confocal microscopy

Optical sections of the three gel samples were obtained using a Leica SP5 confocal microscope (Leica, Wetzlar, Germany) with a HCX PL APO CS 63×, NA 1.2 water immersion objective (Leica) in fluorescence mode. A 543 nm HeNe Laser (1 mW) was used to excite the specimen, and the emitted light of wavelengths between 557 nm and 625 nm was collected. A stack of consecutive image planes with vertical distance d_z was taken for each sample. The vertical spacing was adjusted to $d_z \approx d_{xy}$. The remaining differences between d_z and d_x, d_y were dealt with by linear interpolation to ensure exact cubic voxel size in the three-dimensional data set. The 8-bit grayscale images had 512^2 pixels, with 408, 333, and 458 stacked images for Gel 1 (1.2 mg/mL), 2 (1.6 mg/mL), and 3 (2.4 mg/mL), respectively. The pixel width of the confocal microscopy images, and consequently the voxel width, of the three-dimensional data sets was 0.1 μm for Gel 3 (2.4 mg/mL) and 0.15 μm for the others. Examples of confocal sections for each gel are shown in Fig. 1.

Most digital imaging systems use pixel sizes of ~100 nm for objectives with a numerical aperture between 1.2 and 1.4 (22). This choice is considered to be a good compromise between a maximum utilization of the optical resolution (≈0.25 μm in the lateral direction) and a minimum image file size. For the lateral direction a pixel sizes of 100 nm is close to the Nyquist limit but it can be shown that excessive oversampling, also called empty magnification, would only give a marginal gain in resolution but would lead to larger file sizes and longer computation times (22). Because of the reduced optical resolution in the z direction (≈0.5 μm), a vertical voxel size of 0.25 μm would be sufficient to fulfill the Nyquist criterion; however, our image processing algorithms were optimized for cubic voxels.

Morphological image analysis

The confocal microscopy data sets were converted into binary data sets of the same size by simple threshold segmentation. All voxels with intensity greater than a chosen threshold value I_c were set to 1 (collagen) and all others to 0 (fluid). Before segmentation, a sequence of Gaussian (isotropic) smoothing followed by anisotropic diffusion smoothing (20) was applied to the grayscale data for noise removal. Fig. 2 *a* shows an example of the segmented data set.

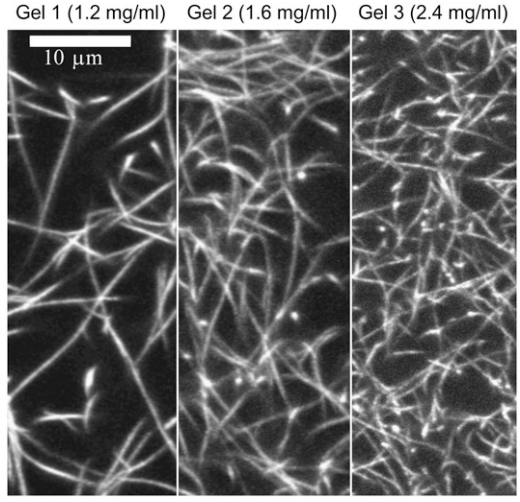

FIGURE 1 Two-dimensional confocal microscopy images of the reconstituted collagen gels analyzed in this study.

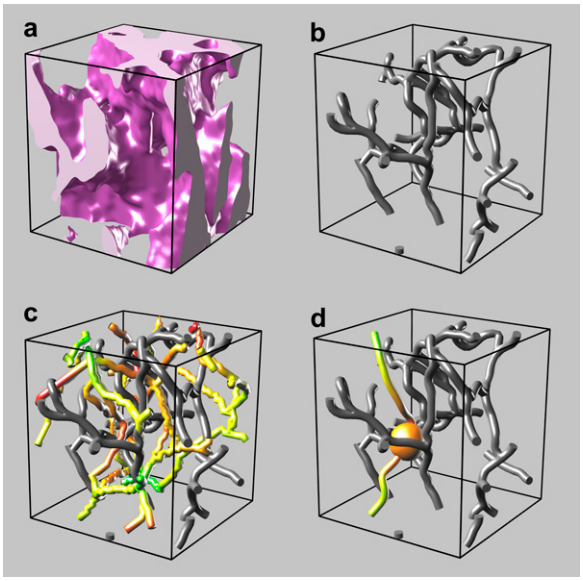

FIGURE 2 Illustration of the three-dimensional image data analysis on a small (5 μm)^3 subset of Gel 3 (2.4 mg/ml). (*a*) Binary data set; all voxels with $I(p) > I_c$ represent the collagen phase. The fiber thickness overestimates the width of collagen fibers (0.15 μm), in particular in the vertical z direction. (*b*) The medial axis of the collagen domain as a one-dimensional curve representation of the fibers. (*c*) Medial axis of the fluid phase, i.e., the complement of the collagen fibers, as a network of widest paths through the collagen matrix. The color indicates the distance to the nearest collagen fiber, with distance increasing from red to blue. (*d*) A single percolating path of the fluid medial axis together with the bottleneck sphere at its point with minimal distance.

The segmented data set contains in general some noise defects, notably isolated fluid voxels or small fluid clusters surrounded by collagen voxels and narrow gaps between collagen fibers that appear to form part of the same fiber. While the classification of these features as defects implies some interpretation, we removed such defects by so-called morphological closing or dilation-erosion (12). This involves dilation of the 1-phase (collagen) by a width R_{DE} (here $R_{DE} = 1$); all voxels of the fluid phase with Euclidean distance less than R_{DE} to the nearest collagen voxel are converted to 1. This is followed by an erosion step in which all voxels of the dilated collagen phase with Euclidean distance less than R_{DE} to the fluid phase are converted to 0. This implies that collagen domains with distance less than or equal to two voxels are merged. The minimum resolved fiber spacing is hence two voxels. In addition, we removed all clusters of the fluid phase that are fully surrounded by the collagen phase.

The collagen phase of the data set obtained by this process overestimates the true diameter of the collagen fibers of ~0.15 μm (7) due to the point-spread function of confocal microscopy systems (23). This broadening is particularly pronounced in the vertical z direction. Therefore, the collagen fibers are better represented as thinned and centered subsets of the 1-phase, called medial axes. The medial axis can be computed by distance-ordered homotopic thinning (24–26). It traces the paths through the center of the collagen fibers and is one-voxel thick. We note that the same algorithm is also well suited for the computation of the medial axis of the fluid phase (see below). An alternative skeletonization algorithm for biopolymer fibers based on tracing maximally wide paths in the Euclidean distance map has been described by Wu et al. (19).

The medial axis is derived from the Euclidean distance map, EDM (27–29), of the 1-phase. The EDM specifies for every voxel of the 1-phase the distance from its center to the center of the nearest voxel of the fluid 0-phase. The EDM is used to thin the collagen phase to its one-voxel-thick medial axis. To do this, voxels of the 1-phase are incrementally converted to 0 in order of their distance values, provided that this conversion does not change the topology and connectivity of the 1-phase. (Note that the resulting medial axis is a 26-connected set of voxels, i.e., the 3^3-neighborhood of each medial axis voxel contains at least one other medial axis voxel, unless the medial axis reduces to a single voxel.)

The medial axis is guaranteed to be homotopy-equivalent to the body represented by the collagen phase and correctly represents its topology. It is also as geometrically centered in the fibers as possible. There are in general many caveats to skeletonization of arbitrary three-dimensional bodies. The geometry of an arbitrary three-dimensional object, including labyrinthine networklike structures (30), cannot in general be represented by a one-dimensional line skeleton (31). However, the geometry of a network structure consisting of connected tubes of convex cross section, possibly with varying but small diameters, is well represented by a one-dimensional medial axis. This includes the collagen networks studied here. For such structures, the medial axis computation is also not sensitive to details of the definition of the skeletonization algorithm or to noise.

All following data are computed from a representation of the collagen fibers as the medial axis of the 1-phase.

We apply two different measures to characterize the width of the pores of the fluid phase between the collagen fibers, namely a pore size distribution and a percolation threshold. Both are computed from the Euclidean distance map of the fluid phase.

The pore size distribution is given by the distribution of values of the covering radius transform (10,11); see Fig. 3. The covering radius transform assigns a value D_f to each voxel of the data set (with subscript f since we apply it to the fluid phase). For a voxel p the positive value $D_f(p)$ is the radius of the largest

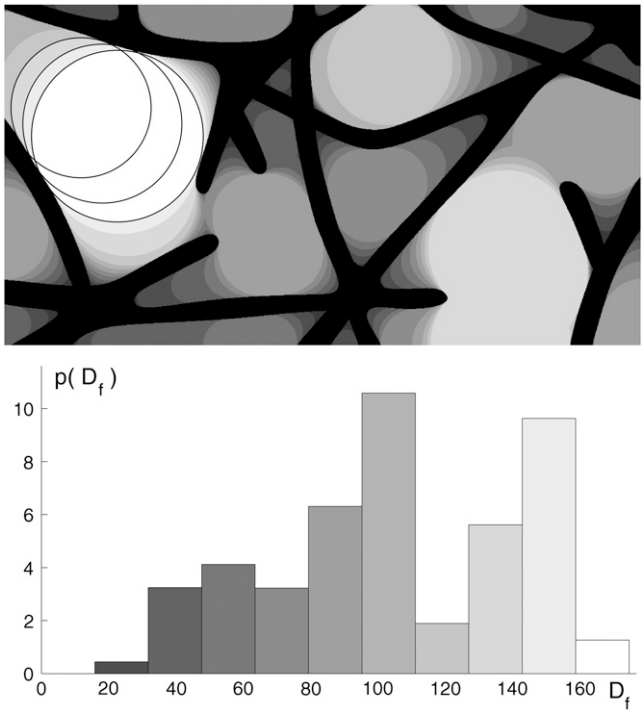

FIGURE 3 Illustration for the maximal covering radius transform of the fluid phase of the collagen network. (*Top*) The image shows a two-dimensional schematic representation of a collagen gel (*black*). The gray-level of each fluid phase pixel corresponds to the maximal covering radius transform value D_f. It represents the radius of the largest sphere fully contained in the fluid phase that covers that pixel. For clarity, the outlines of a few of the maximal disks have been highlighted. The colors in the histogram below provide a bar chart mapping D_f to color. (*Bottom*) The distribution of maximal covering radii (in arbitrary units on the y axis). See Fig. 4 for the distributions of the real collagen network data sets.

EDM sphere centered anywhere in the fluid phase that covers the voxel p. An EDM sphere is a sphere with a radius that corresponds to the Euclidean distance map value at its center point. The distribution $p(D_f)\Delta D_f$ gives the volume that is covered by all EDM spheres of radius $R > D_f$ minus the volume that is covered by all EDM spheres with radius $R > D_f + \Delta D_f$; see Fig. 4. ΔD_f is the bin width of the distribution. The definition of pore size as the average of the covering radius transform corresponds to an incremental filling of the fluid phase by overlapping EDM spheres of decreasing size, starting with the global EDM maximum. (Note that for reasons of digital topology relating to the medial axis computation—specifically to turn the collagen medial axis into a 6- rather than 26-connected object—it is necessary to compute the EDM of the fluid phase for a dilated version of the collagen medial axis, i.e., a dilation of the medial axis by one voxel as described above. This implies a reduction of the EDM values of the fluid phase by one linear voxel size. The results for the pore size distribution of the fluid phase (see Figs. 6 and 7 and the data in Tables 1 and 2) take this additional thickness of the fibers into account and are reduced by one voxel.)

The covering radius pore-size distribution is normalized to the total volume V_f of the fluid phase, i.e., $\int_{r=0}^{\infty} p(r)dr = V_f$. Indeed the EDM spheres that contribute to the distribution, i.e., exactly those that are not fully covered by larger EDM spheres, are so-called maximal balls, in a computational geometric sense. Their centers form the so-called medial surface (30,32–34). The medial surface defines a backbone or skeleton representation of the fluid phase that consists of surface patches rather than one-dimensional lines (30). The medial surface—as opposed to the one-dimensional medial axes considered in this article—allows for the exact reconstruction of the original fluid phase as a union of maximal spheres (34). The medial surface degenerates to a line if the cross section is circular.

A secondary pore size distribution is obtained by the analogous construction but restricted to EDM spheres that are located on the medial axis of the fluid phase, i.e., on the network of maximally wide paths between the fibers (see Fig. 2, *b* and *c*). This distribution is not normalized to the total volume of the fluid phase but instead to the volume of the union of medial axis maximal spheres. We refer to the average of this distribution as $\langle D_{f,MA}\rangle$. This is a relevant measure because the union of maximal spheres centered on the medial axis of the fluid phase represents to a first approximation the possible flow pathways of an intruder particle through the network. This distribution yields larger pore sizes than the full radius covering transform distribution.

A third measure for the pore size of the fluid phase that is directly relevant to the problem of a spherical intruder particle of given radius D is the medial axis percolation threshold D_c evaluated with respect to a given reference direction x, y, or z. The percolation threshold is defined as the radius of the largest sphere that can traverse the fluid phase between the collagen fibers

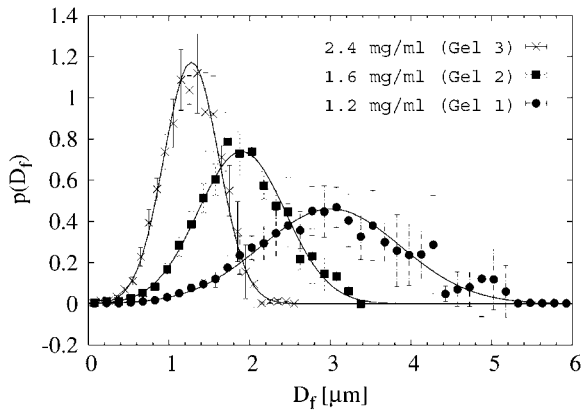

FIGURE 4 Distribution $p(D_f)$ of three-dimensional covering radius transform D_f values of the fluid phase of the three investigated gels for a fixed segmentation parameter of $\Lambda = 70\%$. The lines are normal distributions $(\sigma_f\sqrt{2\pi})^{-1}\exp(-(D_f - \langle D_f\rangle)^2/(2\sigma_f^2))$ with variables σ_f and $\langle D_f\rangle$ from Table 2. The error bars represent the standard deviation of each data point when evaluated on eight subsets arranged on a $2 \times 2 \times 2$ array.

TABLE 1 Morphological characteristics of collagen gels with different concentrations *c*, together with estimates for the systematic error due to changes of the segmentation parameter

	Gel 1 (1.2 mg/ml)	Gel 2 (1.6 mg/ml)	Gel 3 (2.4 mg/ml)
L_S	0.12 ± 0.02	0.22 ± 0.04	0.50 ± 0.06
$\langle D_{f,MA}\rangle$	3.2 ± 0.2	2.3 ± 0.1	1.5 ± 0.1
$\langle D_f\rangle$	3.0 ± 0.1	1.9 ± 0.1	1.3 ± 0.1
D_c	2.8 ± 0.3	1.8 ± 0.2	1.2 ± 0.1

Values for the specific fiber length L_S, average pore sizes $\langle D_f\rangle$ and $\langle D_{f,MA}\rangle$, and percolation threshold D_c are averaged over all data points with segmentation parameter Λ in the interval $I = [0.55, 0.8]$. These averages correspond to the horizontal lines in Figs. 6–9. The percolation threshold D_c is the average $D_c = (D_c^x + D_c^y + D_c^z)/3$. The error estimates $\Delta g = \max\{|g_i - \overline{g}|\}$ for each of these quantities g are the maximal deviation of any of the m data points g_i in I from the average $\overline{g} = \sum g_i/m$. See the text for specific details for L_S. All values are given in μm.

from one side of the data set to the other in the given direction. For example, the percolation threshold D_c^z is the radius of the largest sphere that can traverse the data set from top to bottom.

Modern Euclidean distance map algorithms have linear computational complexity in the number of voxels of the image (29) but with prefactors that are morphology-dependent. The thinning operation for the computation of the medial axis requires a number k of iterations, each proportional to the number of interface voxels between phases 0 and 1. In the worst case, k is the maximal value of the Euclidean distance map. The percolation thresholds are computed by $\log(m)$ fast linear sweeps through the Euclidean distance transform image where m is the maximal Euclidean distance map value divided by the desired precision of the threshold. In a simple implementation, the maximal covering radius transform is determined by l sweeps where l is the maximal Euclidean distance value divided by the increment ΔD_f in sphere sizes.

RESULTS

We analyze the average pore sizes, the percolation threshold, and the specific length of collagen networks for three collagen concentrations. In all cases, these data are found to be approximately constant over a certain range of values of the segmentation parameter and have modest spatial variations throughout the samples.

TABLE 2 Morphological characteristics of collagen gels with different concentrations *c* together with estimates for the statistical error due to the random nature of the media

	Gel 1 (1.2 mg/ml)	Gel 2 (1.6 mg/ml)	Gel 3 (2.4 mg/ml)
L_S	0.12 ± 0.02	0.22 ± 0.02	0.48 ± 0.02
$\langle D_f\rangle$	3.0 ± 0.2	1.90 ± 0.08	1.28 ± 0.05
σ_f	0.8 ± 0.1	0.54 ± 0.05	0.34 ± 0.02
D_c^x	2.7 ± 0.3	1.7 ± 0.1	1.2 ± 0.1
D_c^y	2.6 ± 0.4	1.7 ± 0.1	1.1 ± 0.1
D_c^z	2.5 ± 0.3	1.7 ± 0.1	1.1 ± 0.1
D_χ	2.3 ± 0.3	1.6 ± 0.1	1.2 ± 0.1

These values for the specific fiber length L_S, average pore sizes $\langle D_f\rangle$, and percolation threshold D_c are evaluated for a single segmentation parameter $\Lambda = 0.7$ for data sets of size 300^3 voxels, i.e., $(30\ \mu m)^3$ for Gel 3 and $(45\ \mu m)^3$ for Gels 1 and 2. For the error estimates the sample was subdivided into an array of 2^3 cubic subsets of size 150^3 voxels and g_i was computed for each subset i. The errors are $(\sum_{i=1}^{8}(g_i - g)^2/7)^{1/2})$ with $g = \sum_{i=1}^{8} g_i/8$. All values are given in μm.

We use the integrated intensity Λ of the fluid phase as the segmentation parameter instead of the segmentation threshold I_c (see Fig. 5). For a given segmentation threshold I_c, the integrated intensity of all voxels of the fluid phase is $\Lambda = (\sum I(p))^{-1} \sum^{*} I(p)$, where $I(p)$ is the intensity of voxel p in the original intensity data set, $\sum$ is the sum over all voxels of the data set, and $\sum^{*}$ is the sum over all voxels of the fluid phase. Hence $\Lambda = 0$ corresponds to the limit where all voxels are identified as fluid voxels and $\Lambda = 1$ to the case where all voxels are identified as collagen. For a given segmentation threshold I_c and the corresponding 0-phase (fluid) and 1-phase (collagen), $\Lambda(I_c)$ is the integrated intensity of the fluid phase. Since Λ increases monotonically with I_c, Λ can be used as the relevant parameter of the segmentation process. As an additional advantage, the use of Λ conceals the irrelevant absolute range of the intensity values, for example, 8- or 16-bit intensity resolution or different use of the dynamic range. In practice, one performs the analysis as function of I_c and presents the data as function of Λ.

The key idea—supported by the data presented below—is that the essential large-scale features of the medial axis skeleton of the segmented collagen phase, but not those of the segmented collagen phase itself, are independent of the segmentation parameter Λ over a certain range of Λ. In this range, a change of Λ predominantly affects the apparent width or thickness of the collagen fibers in the segmented data set but not their location or existence.

It is instructive to consider the limits of large and small Λ where this threshold independence breaks down: The average pore size, shown in Figs. 6 and 7 as a function of Λ, increases sharply for small and large values of Λ. The increase for large Λ is due to loss of fibers with small fluorescence signal. The increase for small values of Λ is due to merging of distinct fibers as the fluid phase between them is erroneously identified as collagen. Nevertheless, there is an intermediate regime where a change in the segmentation parameter affects predominantly the thickness of the fibers but only marginally their position or existence. This intermediate range was $0.55 \leq \Lambda < 0.8$ for the collagen data sets but needs to be assessed individually for each material.

The percolation threshold was also found to be approximately constant over the same range of Λ (Fig. 8). In addition, there was no statistically significant difference between the horizontal (x,y) and the vertical direction (z) through the sample. The same data presented in Fig. 8 with the collagen fibers represented by the 1-phase of the segmented data set instead of its medial axis show large Λ-dependent differences between D_c^x and D_c^z (data not shown) that are certainly partly due to anisotropic point-spread function of the imaging system. The medial axis representation reduces the anisotropy artificially introduced by the imaging system.

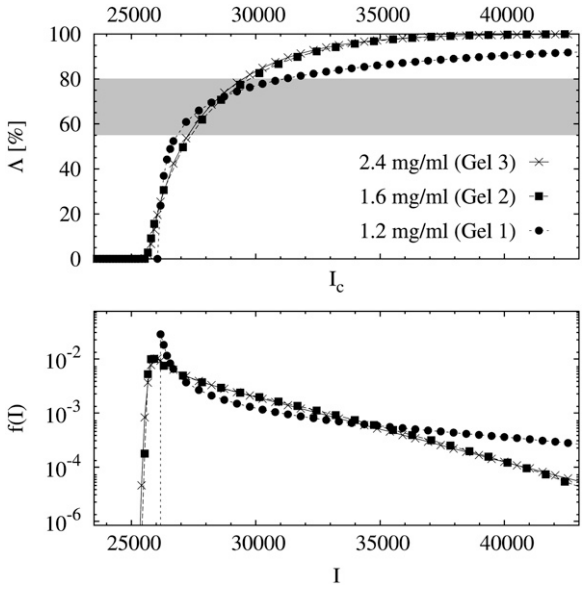

FIGURE 5 Intensity distribution $f(I)$ of the confocal image stacks (*bottom*) and cumulative sum $\Lambda(I) = \int_0^I f(I')dI'$ (*top*). The gray bar corresponds to values of Λ, and according values for the segmentation threshold I_c, for which the pore size characteristics are almost constant.

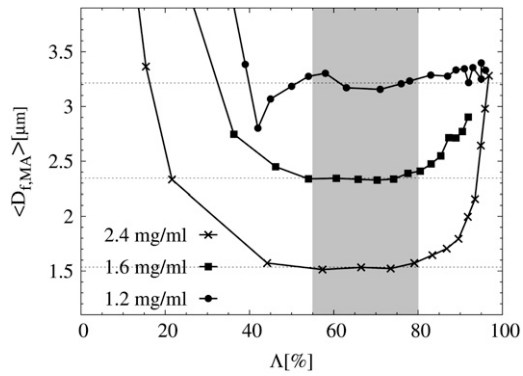

FIGURE 6 Average $\langle D_{f,MA} \rangle$ of the covering radius pore size distributions of the fluid phase as function of the segmentation parameter Λ, restricted to EDM spheres on the medial axis. For an intermediate range of Λ (*shaded region*), $\langle D_{f,MA} \rangle$ is nearly constant. These data were evaluated on a subset of approximate size $(17\ \mu m)^3$ for Gel 3 and $(25\ \mu m)^3$ for Gels 1 and 2.

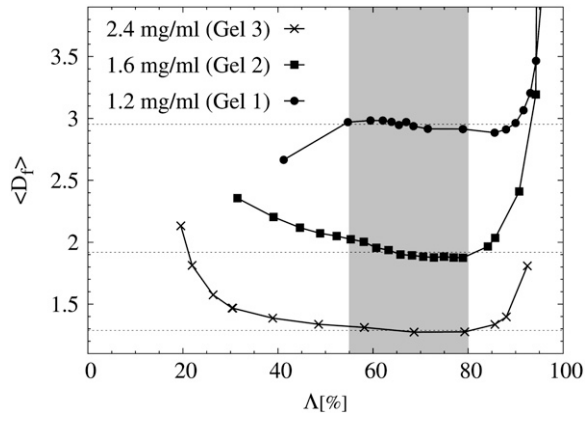

FIGURE 7 Average $\langle D_f \rangle$ of the covering radius pore size distributions of the fluid phase as function of the segmentation parameter Λ incorporating the whole fluid phase as described in Fig. 3. These data are evaluated on a subset of size 280^3 voxels.

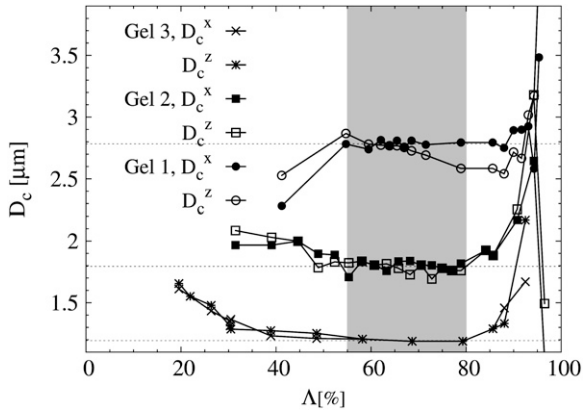

FIGURE 8 The percolation threshold of the fluid phase as function of the segmentation parameter Λ, for the vertical (Z) and for one of the horizontal (x) directions. The straight lines are linear fits to the data points in the interval $0.55 \leq \Lambda \leq 0.8$ for the horizontal direction. The percolation threshold for the y direction is up to statistical deviations the same as x (data not shown).

Note that the average pore size $\langle D_f \rangle$ of the fluid phase and the percolation threshold D_c are similar. This finding points toward a spatial homogeneity of the collagen networks. The width of the bottleneck along the single, maximally widest path through the network is approximately equal to the integral quantity $\langle D_f \rangle$.

Fig. 9 shows the specific length L_S, i.e., total fiber length of the network divided by the total volume of the data set as function of Λ. In contrast to the pore size or percolation thresholds, the length is sensitive to small-scale details of the medial axis and its discretization and to additional image processing steps, such as pruning of dangling dead-ends of the medial axis. The error estimates for L_S in Table 1 correspond to variations of L_S with Λ and to differences depending on the level of smoothing applied to the piecewise linear representation of the medial axis before measuring its length. We unexpectedly found L_S to increase disproportionally with increasing collagen concentration. It suggests that at higher collagen concentrations the fiber diameter is smaller (a rather

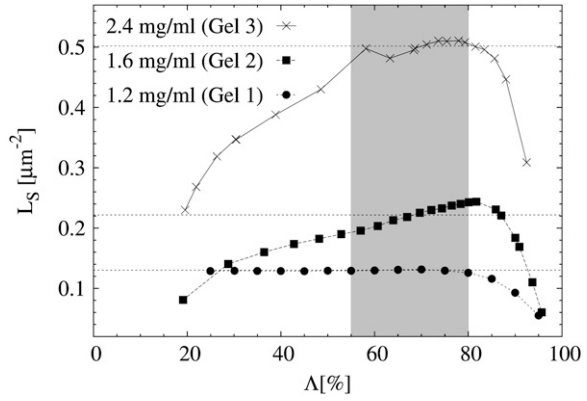

FIGURE 9 Specific length, i.e., length/volume, of the collagen fiber network as function of segmentation parameter Λ.

unlikely scenario) or that the polymerization efficiency (the fraction of polymerized to unpolymerized collagen) was higher.

The computational effort necessary to compute all quantities as function of the threshold parameter Λ is not prohibitive. Nevertheless, for additional analyses, such as error or homogeneity estimates or the analysis of sequences of similar data sets, it may be useful to extract a value for an optimal segmentation threshold. While there is no universal system-independent value for an optimal threshold Λ_c, a value approximately centered in the range of Λ where the morphological measures only vary mildly is a sensible choice. Specifically for the collagen data we choose $\Lambda_c = 0.7$.

The errors of the intrinsic morphological measures that stem from the irregular or disordered nature of the media can be determined by analyzing subsets of the data. These provide an indication of whether the sample size was sufficiently large. The value g_a of a morphological measure g is computed for a cubic subset of the data chosen maximally large but sufficiently smaller than the whole data set to exclude boundary effects, (30 μm)^3 for Gel 3 and (45 μm)^3 for Gels 1 and 2. This subset is then subdivided into a grid of n^3 cubic subsets (here $n = 2$), for each of which the value g_i with $i = 1, \ldots, n^3$ of g is computed. For an intensive measure, g_a equals $g'_a = 1/n^3 \sum_i^{n^3} g_i$ by definition and $\Delta g = \left(\sum_{i=1}^{n^3} (g_i - g_a)^2/(n^3 - 1)\right)$ is an appropriate estimate for the error due to the statistical nature of the system.

Table 2 shows the results of this analysis demonstrating that the sizes of the collagen data sets were sufficient relative to the inhomogeneity of the collagen network. This analysis was carried out for a fixed segmentation parameter $\Lambda = 0.7$. The importance to quantify both this statistical error (Table 2) and the systematic error due to changes of the segmentation parameters (Table 1) is demonstrated by the specific length; for L_S the statistical error evaluated for a single Λ is small but the systematic error associated with variations of Λ and other process parameters is large.

In addition, Fig. 4 shows the distributions of $\langle D_f \rangle$ for $\Lambda = 0.7$. These data suggest that these distributions are approximately given by normal distributions $(\sigma_f \sqrt{2\pi})^{-1} \exp(-D_f - \langle D_f \rangle)^2/(2\sigma_f^2)$ with values of σ_f and $\langle D_f \rangle$ tabulated in Table 2.

We have also validated the robustness of our method against noise for simple synthetic data sets. To this end we have generated a synthetic confocal microscopy data set by convoluting the medial axis representation of Gel 2 with an approximation of a typical point-spread function and application of Gaussian smoothing. Furthermore we have added additive uncorrelated noise with a given amplitude $r/\Delta I$ to the grayscale data set before computing the average pore size $\langle D_f \rangle$ by the same process as described above. ΔI is the standard deviation of the distribution of intensities in the grayscale data set. The values for the average pore size $\langle D_f \rangle$ obtained from the original network model and from the grayscale data set by application of the methods described are the same, as expected. Fig. 10 shows that $\langle D_f \rangle$ as a function of

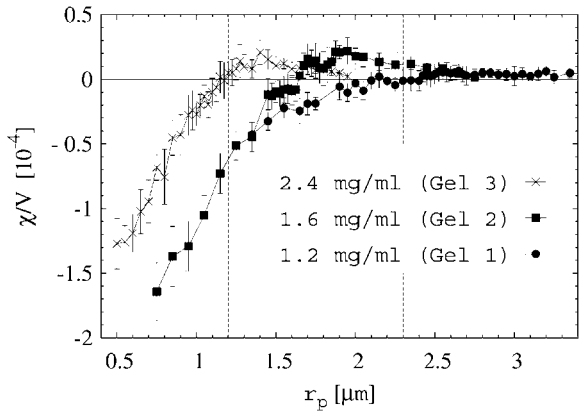

FIGURE 10 The Euler index of dilated versions of the collagen network as a function of the dilation radius. The vertical lines mark the dilation radius D_χ for which χ vanishes.

Λ is indeed almost constant in the absence of noise and that our method is robust against strong levels of uncorrelated noise (e.g., $r/\Delta I = 4$).

Relation of the percolation threshold to the Euler index

The percolation threshold, defined above, has thus far been used as a collagen pore size measure. However, percolation thresholds are of broader importance including applications to transport in random media (35–37). We show that our data are commensurate with a hypothesis linking the percolation threshold D_c to the Euler index, a fundamental topological quantity (38).

For the collagen networks the percolation threshold D_c marks a critical size of a spherical intruder particle, in the sense that smaller particles can migrate globally through the whole fluid phase whereas larger particles are confined to local domains of the medium. More generally, percolation thresholds always mark the parameter value for a random system where isolated clusters merge to form percolating domains that extend through the whole available space. (35,36). This implies the relevance of percolation thresholds to global physical properties of heterogeneous media.

The Euler index χ is a fundamental morphological descriptor of the topology and connectivity of spatial structure. The Euler index is defined by integral geometry (39,40). For a three-dimensional solid body $K \in \mathbb{E}^3$ it is given by $\chi = N - R + C$ where N is the number of connected components of K, R the number of handles, and C the number of hollow cavities (holes) in K (39). It is hence a topological quantity (i.e., remains constant if the body is deformed unless the deformation includes cutting or gluing). The computation of the Euler index of the 1-phase of a voxelized data set is a fast local linear-time procedure (40).

Note that the Gauss-Bonnet theorem (41) states that χ is also given by the integral of the Gaussian curvature G over bounding surface $S = \partial K$, that is $\chi = (4\pi)^{-1} \int_S G(p)dp$. It is important to accurately state if one computes the Euler characteristic χ of the body K or the Euler characteristic χ_S of its bounding surface $S := \partial K$. For a three-dimensional solid body K the relation $\chi = \chi_S/2$ holds. This is derived by considering that $\chi(K^c) = -(-1)^d\chi(K)$ for any d-dimensional body K and its compactified complement $K^c = (\mathbb{E}^3 \backslash K) \cup \partial(\mathbb{E}^3 \backslash K)$. Applying the additivity relation $\chi(K_1 \cup K_2) = \chi(K_1) + \chi(K_2) - \chi(K_1 \cap K_2)$ (that is valid for any K_1 and K_2) to $K_1 = K$ and $K_2 = K^c$ yields with $\partial K = K_1 \cap K_2$ and $\chi(K_1 \cup K_2 = \mathbb{E}^3) = 0$ that the Euler characteristic of the bounding surface is $\chi(\partial K) = \chi(K)/2$ (39).

The Euler index has been shown to be a relevant descriptor of global properties of spatial patterns for a variety of physical problems and relevant for percolation transitions (42). Indeed it was conjectured that for a wide class of random structure models the percolation thresholds are bounded tightly from above by the zero of the mean Euler index (38). Although not proven rigorously, numerical studies of various different types of percolation models suggest that the analysis of the Euler index provides an estimate of the percolation threshold (43,44). The random homogeneous nature of the material is essential for this conjecture as it is trivial to construct counter-examples, for example by superposing a smaller-scale porous structure on the solid phase, which greatly changes χ but does not affect the percolation threshold.

A dilation $K_c(r_p)$ of the collagen network with dilation radius r_p is the set of voxels that are closer to the medial axis representing the collagen fibers than r_p. The value of the dilation radius for which the Euler index of the dilated collagen network vanishes, $\chi(D_\chi) = 0$, is denoted D_χ. The complement $K_f(r_p)$ of the dilated collagen network is the space in which the centers of spheres of radius r_p can move. If K_f is (not) percolating for a given radius r_p, then a sphere of radius r_p can (cannot) traverse the collagen network. Note that the Euler characteristics of K_c and of its complement K_f are the same except for effects due to the sample boundary.

Fig. 11 shows the Euler index $\chi(r_p)$ of dilations of the collagen network as function of the dilation radius r_p. These data support the hypothesis that the zero of the Euler index at D_χ is close to the percolation threshold D_c, considering the statistical errors. The values of D_χ are smaller than D_c (see Tables 1 and 2), consistent with the statement that D_χ is an upper bound for the percolation threshold of the fluid phase. This finding lends additional experimental support to the hypothesis that the percolation threshold of sufficiently homogeneous disordered materials is related to the topology of the material.

CONCLUSION

We have presented a method for extracting morphological measures of reconstituted collagen networks—in particular, pore-size distributions and percolation thresholds—from confocal microscopy image stacks. This method is robust

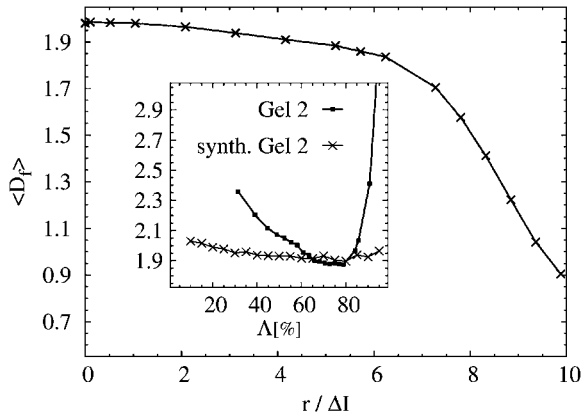

FIGURE 11 Analysis of the noise sensitivity of $\langle D_f \rangle$ for a simulated collagen data. The grayscale data set is obtained from a binary data set representing the medial axis of Gel 2 with $\Lambda = 70\%$ by convolution with a representation of the point-spread function and application of Gaussian smoothing. The inset shows $\langle D_f \rangle$ as a function of the integrated intensity Λ, demonstrating that for such an idealized situation $\langle D_f \rangle$ is almost constant over a much larger range of Λ than for the experimental data sets. For comparison, the data for the real data set of Gel 2 from Fig. 7 are also shown. The main plot shows $\langle D_f \rangle$ for the simulated data set with $\Lambda = 0.7$ as a function of the strength of white noise, i.e., random numbers between $[-r/\Delta I, r/\Delta I]$ are added to the intensity values of each pixel where ΔI is the standard deviation of the distribution of intensities of the unperturbed data set.

against variations of the segmentation parameter Λ that is used to segment the grayscale intensity images. The key idea is to derive morphological measures from the medial axes of the collagen phase or the fluid phase and to use the robust average of the maximal covering radius transform as pore size estimate. The measurements described here exploit the three-dimensional nature of the confocal microscopy data set. Our analysis of the concentration-dependence of the average pore size is consistent with previously published data (13).

We also provide empirical support for the recent conjecture that the percolation critical lengths D_c are well approximated by the zeros as function of r_p of the Euler index χ of the dilated collagen network body with dilation radius r_p.

The presented method of pore size characterization is not limited to collagen networks but can be applied to any fibrous polymer network such as bundled F-actin, fibrin, cytoskeletal filament networks, etc., as long as the individual fibers can be resolved by the confocal imaging system. Fast confocal scanning microscopy has become a widely used tool in cell biology for live-cell imaging of cytoskeletal filaments in three dimensions. Moreover, using video-rate confocal super resolution (stimulated emission depletion) microscopy, the three-dimensional live-cell imaging of cortical actin structures with their typical mesh size of <200 nm should become possible in the near future (45,46).

The average pore size and the percolation threshold of less than 3 μm for all three collagen concentrations investigated indicate that these collagen networks form a steric barrier against the invasion of cells (3). The fact that many tumor cells can easily migrate through these collagen networks (5) suggest that they must employ mechanisms to overcome the steric hindrance of the matrix, such as proteolytic collagen degradation or the generation of protrusive forces that deform and widen the network pores (3). For a quantitative understanding of cell migration through such three-dimensional networks, a characterization of their morphological properties is therefore essential.

The fiber width of the analyzed collagen samples corresponds approximately to the voxel size and is known to be almost constant. This is the simplest situation for the methods presented but not a requirement. The average $\langle D_f \rangle$ of the maximal covering radius transform is a robust pore size measure for any reliable voxelized representation of the fluid phase. The representation of the fiber network as the medial axis is immediately applicable to a network of circular fibers with arbitrary constant fiber thickness; the medial axis is simply dilated to the known radius of the fibers. If the fiber cross section varies, a medial axis representation is still possible—with dilation by spatially varying radii—but the dependence of $\langle D_f \rangle$ of the segmentation parameter Λ is more complex; thinner fibers have lower intensities and a change in Λ does not only affect the fiber width but also the network composition (relevant, for example, for biopolymer networks in the presence of bundling proteins). For thick fiber networks, the medial axis representation is unnecessary as the solid phase can be obtained by deconvolution with the point-spread function.

In summary, the medial axis approach, combined with the maximal covering radius transform as a pore-size measure, facilitates the robust and quantitative analysis of the morphology of three-dimensional filamentous networks from diffraction-limited noisy confocal images. The approach applies similarly to other robustly defined morphological descriptors (such as integral measures of fiber orientation) and can, in principle, be extended to noise-sensitive measures such as branching ratios or branching angles.

We thank Christoph Arns (University of New South Wales, Sydney, Australia) for useful discussions regarding the maximal covering radius transform. We are grateful to the Australian Partnership for Advanced Computing for generous allocation of CPU time.

We acknowledge support by the Deutsche Forschungsgemeinschaft through grant Nos. SCHR 1148/2-1 and FA 336/2-1, by the National Institutes of Health through grant No. HL65960, and by the German Academic Exchange Service (DAAD) for travel to Boston, MA, and Canberra, Australia. L.M.J., D.A.V., and D.A.W. were supported by the National Science Foundation (grant Nos. DMR-0602684 and CTS-0505929) and the Harvard Materials Research Science and Engineering Center (grant No. DMR-0820484).

REFERENCES

1. Cukierman, E., R. Pankov, D. Stephens, and K. Yamada. 2001. Taking cell-matrix adhesion to the third dimension. *Science*. 294:1708–1712.
2. Pedersen, J., and M. Swartz. 2005. Mechanobiology in the third dimension. *Ann. Biomed. Eng*. 33:1469–1490.
3. Zaman, M., L. Trapani, A. Siemeski, D. Mackellar, H. Gong, R. Kamm, A. Wells, D. Lauffenburger, and P. Matsudaira. 2006. Migration of tumor

cells in 3D matrices is governed by matrix stiffness along with cell-matrix adhesion and proteolysis. *Proc. Natl. Acad. Sci. USA.* 103:10889–10894.

4. Wolf, K., I. Mazo, H. Leung, K. Engelke, U. von Andrian, E. Deryugina, A. Strongin, E. Brocker, and P. Friedl. 2003. Compensation mechanism in tumor cell migration: mesenchymal-amoeboid transition after blocking of pericellular proteolysis. *J. Cell Biol.* 160:267–277.
5. Mierke, C., D. Paranhos-Zitterbart, P. Kollmannsberger, C. Raupach, U. Schlötzer-Schrehardt, T. Goecke, J. Behrens, and B. Fabry. 2008. Breakdown of the endothelial barrier function in tumor cell transmigration. *Biophys. J.* 94:2832–2846.
6. Parkhurst, M., and W. Saltzman. 1992. Quantification of human neutrophil motility in three-dimensional collagen gels. Effect of collagen concentration. *Biophys. J.* 61:306–315.
7. Kuntz, R., and W. Saltzman. 1997. Neutrophil motility in extracellular matrix gels: mesh size and adhesion affect speed of migration. *Biophys. J.* 72:1472–1480.
8. Ranucci, C., A. Kumar, S. Batra, and P. Moghe. 2000. Control of hepatocyte function on collagen foams: sizing matrix pores toward selective induction of 2D and 3D cellular morphogenesis. *Biomaterials.* 21:783–793.
9. Gardel, M., J. Shin, F. MacKintosh, L. Mahadevan, P. Matsudaira, and D. Weitz. 2004. Elastic behavior of cross-linked and bundled actin networks. *Science.* 304:1301–1305.
10. Hazlett, R. 1995. Simulation of capillary-dominated displacements in microtomographic images of reservoir rocks. *Transp. Porous Media.* 20:21–35.
11. Thovert, J.-F., F. Yousefian, P. Spanne, C. G. Jacquin, and P. M. Adler. 2001. Grain reconstruction of porous media: application to a low-porosity Fontainebleau sandstone. *Phys. Rev. E Stat. Nonlin. Soft Matter Phys.* 63:061307.
12. Soille, P. 1999. Morphological Image Analysis—Principles and Applications. Springer-Verlag, Berlin, Germany.
13. Saltzman, W., M. Radomsky, K. Whaley, and R. Cone. 1994. Antibody diffusion in human cervical mucus. *Biophys. J.* 66:508–515.
14. Takahashi, A., R. Kita, T. Shinozaki, K. Kubota, and M. Kaibara. 2003. Real space observation of three-dimensional network structure of hydrated fibrin gel. *Colloid Polym. Sci.* 281:832–838.
15. Kaufman, L., C. Brangwynne, K. Kasza, E. Filippidi, V. Gordon, T. Deisboeck, and D. Weitz. 2005. Glioma expansion in collagen *i* matrices: analyzing collagen concentration-dependent growth and motility patterns. *Biophys. J.* 89:635–650.
16. Schmidt, C., M. Baermann, G. Isenberg, and E. Sackmann. 1989. Chain dynamics, mesh size, and diffusive transport in networks of polymerized actin: a quasielastic light scattering and microfluorescence study. *Macromolecules.* 22:3638–3649.
17. Lindquist, W., A. Venkatarangan, J. Dunsmuir, and T. Wong. 2000. Pore and throat size distributions measured from synchrotron x-ray tomographic images of Fontainebleau sandstones. *J. Geophys. Res.* 105:21509–21527.
18. Zhou, Y., A. Kaufman, and A. Toga. 1998. Three-dimensional skeleton and centerline generation based on an approximate minimum distance field. *Vis. Comput.* 14:303–314.
19. Wu, J., B. Rajwa, D. Filmer, C. Hoffmann, B. Yuan, C. Chiang, J. Sturgis, and J. Robinson. 2003. Automated quantification and reconstruction of collagen matrix from 3D confocal datasets. *J. Microsc.* 210:158–165.
20. Frangakis, A., and R. Hegerl. 2001. Noise reduction in electron tomographic reconstructions using nonlinear anisotropic diffusion. *J. Struct. Biol.* 135:41–44.
21. Baici, A., G. Cohen, K. Fehr, and A. Böni. 1980. A handy assay for collagenase using reconstituted fluorescein-labeled collagen fibrils. *Anal. Biochem.* 108:230–232.
22. Inoué, S., and K. Spring. 1997. Video Microscopy: The Fundamentals, 2nd Ed. Springer, New York.
23. Semwogerere, D., and E. Weeks. 2005. Confocal microscopy. *In* Encyclopedia of Biomaterials and Biomedical Engineering. G. Wnek, and G. Bowlin, editors. Taylor and Francis, New York.
24. Pudney, C. 1998. Distance-ordered homotopic thinning: a skeletonization algorithm for 3D digital images. *Comput. Vis. Image Underst.* 72:404–413.
25. Ma, C., and M. Sonka. 1996. A fully parallel 3D thinning algorithm and its applications. *Comput. Vis. Image Underst.* 64:420–433.
26. Lee, T., R. Kashyap, and C. Chu. 1994. Building skeleton models via 3D medial surface/axis thinning algorithms. *CVGIP: Graph. Models Image Proc.* 56:462–478.
27. Danielsson, P. 1980. Euclidean distance mapping. *Comput. Graph. Image Proc.* 14:227–248.
28. Saito, T., and J. Toriwaki. 1994. New algorithms for Euclidean distance transformation of an *n*-dimensional digitized picture with applications. *Pattern Recognit.* 27:1551–1565.
29. Cuisenaire, O., and B. Macq. 1999. Fast Euclidean distance transformation by propagation using multiple neighborhoods. *Comput. Vis. Image Underst.* 76:163–172.
30. Schröder, G., S. Ramsden, A. Christy, and S. Hyde. 2003. Medial surfaces of hyperbolic structures. *Eur. Phys. J. B.* 35:551–564.
31. Siddiqi, K., and S. Pizer, editors. 2007. Medial Representations: Mathematics, Algorithms and Applications. Springer, New York.
32. Blum, H. 1964. A transformation for extracting new descriptors of shape. *In* Models for the Perception of Speech and Visual Form. W. Wathen-Dunn, editor. The M.I.T. Press, Cambridge, MA.
33. Nackman, L. R. 1982. Curvature relations in three-dimensional symmetric axes. *Comput. Graph. Image Proc.* 20:43–57.
34. Wolter, F.-E. 1992. Cut locus and medial axis in global shape interrogation and representation. MIT Design Laboratory Memorandum 92–2, Massachusetts Institute of Technology, Cambridge, MA.
35. Isichenko, M. B. 1992. Percolation, statistical topography, and transport in random media. *Rev. Mod. Phys.* 64:961–1043.
36. Stauffer, D., and A. Aharony. 1994. Introduction to Percolation Theory, 2nd Ed. Taylor and Francis, New York.
37. Arns, C. 2002. The influence of morphology on physical properties of reservoir rocks. PhD thesis, University of New South Wales, Australia.
38. Mecke, K., and H. Wagner. 1991. Euler characteristic and related measures for random geometric sets. *J. Stat. Phys.* 64:843–850.
39. Santaló, L. 1976. Integral Geometry and Geometric Probability. Addison-Wesley, Reading, MA.
40. Arns, C. H., M. A. Knackstedt, W. V. Pinczewski, and K. R. Mecke. 2001. Euler-Poincaré characteristics of classes of disordered media. *Phys. Rev. E Stat. Nonlin. Soft Matter Phys.* 63:031112.
41. Do Carmo, M. 1976. Differential Geometry of Curves and Surfaces. Prentice Hall, Englewood Cliffs, NJ.
42. Mecke, K. 1998. Integral geometry and statistical physics. *Int. J. Mod. Phys. B.* 12:861–899.
43. Mecke, K., and S. Seyfried. 2002. Strong dependence of percolation thresholds on polydispersity. *Europhys. Lett.* 58:28–34.
44. Neher, R., K. Mecke, and H. Wagner. 2008. Topological estimation of percolation thresholds. *J. Stat. Mech. Theory Exp.* 2008:P01011. http://stacks.iop.org/1742–5468/2008/P01011.
45. Hartwig, J., and P. Shevlin. 1986. The architecture of actin filaments and the ultrastructural location of actin-binding protein in the periphery of lung macrophages. *J. Cell Biol.* 103:1007–1020.
46. Westphal, V., S. Rizzoli, M. Lauterbach, D. Kamin, R. Jahn, and S. Hell. 2008. Video-rate far-field optical nanoscopy dissects synaptic vesicle movement. *Science.* 320:246–249.